AMERICAN SOCIETY FOR MICROBIOLOGY | Infection and Immunity

All Three TonB Systems Are Required for *Vibrio vulnificus* CMCP6 Tissue Invasiveness by Controlling Flagellum Expression

Tra-My Duong-Nu,[a,b] Kwangjoon Jeong,[a,c] Seol Hee Hong,[a,d] Hong-Vu Nguyen,[e] Van-Hoan Ngo,[a] Jung-Joon Min,[e] Shee Eun Lee,[a,d] Joon Haeng Rhee[a,c]

Clinical Vaccine R&D Center, Chonnam National University, Gwangju, Republic of Korea[a]; Department of Molecular Medicine, Graduate School, Chonnam National University, Gwangju, Republic of Korea[b]; Department of Microbiology, Chonnam National University Medical School, Gwangju, Republic of Korea[c]; Department of Pharmacology and Dental Therapeutics, School of Dentistry, Chonnam National University, Gwangju, Republic of Korea[d]; Department of Nuclear Medicine, Chonnam National University Medical School, Gwangju, Republic of Korea[e]

TonB systems actively transport iron-bound substrates across the outer membranes of Gram-negative bacteria. *Vibrio vulnificus* CMCP6, which causes fatal septicemia and necrotizing wound infections, possesses three active TonB systems. It is not known why *V. vulnificus* CMCP6 has maintained three TonB systems throughout its evolution. The TonB1 and TonB2 systems are relatively well characterized, while the pathophysiological function of the TonB3 system is still elusive. A reverse transcription-PCR (RT-PCR) study showed that the *tonB1* and *tonB2* genes are preferentially induced *in vivo*, whereas *tonB3* is persistently transcribed, albeit at low expression levels, under both *in vitro* and *in vivo* conditions. The goal of the present study was to elucidate the raison d'être of these three TonB systems. In contrast to previous studies, we constructed in-frame single-, double-, and triple-deletion mutants of the entire structural genes in TonB loci, and the changes in various virulence-related phenotypes were evaluated. Surprisingly, only the *tonB123* mutant exhibited a significant delay in killing eukaryotic cells, which was complemented in *trans* with any TonB operon. Very interestingly, we discovered that flagellum biogenesis was defective in the *tonB123* mutant. The loss of flagellation contributed to severe defects in motility and adhesion of the mutant. Because of the difficulty of making contact with host cells, the mutant manifested defective RtxA1 toxin production, which resulted in impaired invasiveness, delayed cytotoxicity, and decreased lethality for mice. Taken together, these results indicate that a series of virulence defects in all three TonB systems of *V. vulnificus* CMCP6 coordinately complement each other for iron assimilation and full virulence expression by ensuring flagellar biogenesis.

Vibrio vulnificus is a halophilic estuarine pathogen that causes fatal septicemia and necrotizing wound infections in patients suffering from hepatic diseases with high levels of circulating iron or who are immunocompromised (1–5). Infection with *V. vulnificus* typically shows rapid progression and mortality rates greater than 50% (6, 7). In Gram-negative bacteria, the inner membrane protein complex TonB plays a crucial role in the uptake of iron (8, 9), which is an important micronutrient for numerous biological processes (10–12). TonB complexes transduce the proton motive force (PMF) of the cytoplasmic membrane to energize iron-siderophore complex transport through a specific TonB-dependent transporter (TBDT) across the outer membrane (OM) (9, 13, 14). This system's known biological roles had been restricted to iron complexes (15, 16) and vitamin B_{12} (14), but recent experimental evidence of the TonB-energized transport of nickel and various carbohydrates suggests that the number and variety of TonB-dependent substrates have been underestimated (17–19). Unlike the single TonB system in *Escherichia coli* (8), the genomes of *Vibrio* species carry multiple TonB systems. Interestingly, three TonB systems were first reported in *V. vulnificus* CMCP6 by the late Jorge Crosa's team (20). As a result of the pivotal findings of Crosa's group, the importance of TonB1 and TonB2 systems in the iron transport of siderophores and in the pathogenesis of *V. vulnificus* has been highlighted (20, 21). Also, they reported that the functionally elusive TonB3 has a unique regulation mechanism consisting of Lrp (L-leucine responsive protein) and CRP (cAMP receptor protein) (20, 22). Based upon the regulation of TonB3 system by Lrp and CRP, they proposed that TonB3 would function to integrate different environmental signals such as glucose starvation and the transition between "feast" and "famine." However, the pathophysiological function of TonB3 remains poorly defined. Our preliminary real-time reverse transcription-PCR (RT-PCR) experiments demonstrated that while the *tonB1* and *tonB2* systems are highly expressed *in vivo*, *tonB3* is persistently transcribed, albeit at low expression levels, under *in vitro* and *in vivo* conditions. This result prompted us to study why *V. vulnificus* CMCP6 has maintained three TonB systems throughout the long path of evolution. In previous studies performed by Crosa's group, they used in-frame deletion mutants of the structural *tonB* genes with in *trans* complementation. Since the three TonB systems share similarly functioning genes, single-gene-mutation studies might not rule out the interaction among remaining genes in the same operon and the *tonB* genes in other TonB operons.

Received 23 June 2015 **Returned for modification** 31 July 2015
Accepted 24 October 2015

Accepted manuscript posted online 2 November 2015

Citation Duong-Nu T-M, Jeong K, Hong SH, Nguyen H-V, Ngo V-H, Min J-J, Lee SE, Rhee JH. 2016. All three TonB systems are required for *Vibrio vulnificus* CMCP6 tissue invasiveness by controlling flagellum expression. Infect Immun 84:254–265. doi:10.1128/IAI.00821-15.

Editor: S. M. Payne

Address correspondence to Shee Eun Lee, selee@chonnam.ac.kr, or Joon Haeng Rhee, jhrhee@chonnam.ac.kr.

Supplemental material for this article may be found at http://dx.doi.org/10.1128/IAI.00821-15.

TABLE 1 Strains and plasmids used in this study

Strain or plasmid	Description[a]	Source or reference
Strains		
V. vulnificus		
CMCP6	Wild type, clinical isolate	CNU Hospital
Δ*tonB1*	CMCP6 with in-frame deletion of entire structural genes in TonB1 locus	This study
Δ*tonB2*	CMCP6 with in-frame deletion of entire structural genes in TonB2 locus	This study
Δ*tonB3*	CMCP6 with in-frame deletion of entire structural genes in TonB3 locus	This study
Δ*tonB12*	CMCP6 with in-frame double deletion of entire structural genes in TonB12 loci	This study
Δ*tonB13*	CMCP6 with in-frame double deletion of entire structural genes in TonB13 loci	This study
Δ*tonB23*	CMCP6 with in-frame double deletion of entire structural genes in TonB23 loci	This study
Δ*tonB123*	CMCP6 with in-frame triple deletion of entire structural genes in TonB123 loci	This study
E. coli		
DH5α	F^- *recA1* restriction negative	Laboratory collection
SY327 λ *pir*	Δ(*lac pro*) *argE*(Am) *rif nalA recA56* λ *pir* lysogen	26
SM10 λ *pir*	*thi thr leu tonA lacY supE recA*::RP4-2-Tc^r::Mu Km^r λ *pir* lysogen	26
Plasmids		
pDM4	Suicide vector with ori R6K *sacB*; Cm^r	58
pLAFR3	IncP cosmid vector; Tc^r	59
pRK2013	IncP Km^r Tra $Rk2^+$ *repRK2 repE1*	60
pCMM1509	pDM4 with a 2-kb SacI/SpeI in-frame deleted *tonB1* operon	This study
pCMM1510	pDM4 with a 2-kb SacI/SpeI in-frame deleted *tonB2* operon	This study
pCMM1511	pDM4 with a 1.9-kb SacI/SmaI in-frame deleted *tonB3* operon	This study
pCMM1512	pLAFR3 with a 25-kb fragment containing the in-frame deleted *tonB1* operon	This study
pCMM1513	pLAFR3 with a 25-kb fragment containing the in-frame deleted *tonB2* operon	This study
pCMM1514	pLAFR3 with a 25-kb fragment containing the in-frame deleted *tonB3* operon	This study

[a] Cm^r, Cm resistance; Tc^r, Tc resistance; Ap^r, Ap resistance; Km^r, Km resistance.

Hence, in this study, we constructed mutants with single and multiple deletions of the entire structural genes in TonB loci and complemented them with cosmid clones harboring each operon to evaluate the pathogenic significance of these TonB systems in *V. vulnificus*. Through a variety of experimental approaches, we demonstrated that all three TonB systems appear to coordinately complement each other for flagellum biogenesis and full virulence expression of *V. vulnificus* CMCP6 *in vivo*.

MATERIALS AND METHODS

Bacterial strains, plasmids, and media. The *V. vulnificus* strains, *E. coli* strains, and plasmids that were used in this study are listed in Table 1. The wild-type *V. vulnificus* strain was CMCP6, a highly virulent clinical isolate whose genome sequence was recently reannotated for higher accuracy (23, 24). *E. coli* and *V. vulnificus* were grown in Luria-Bertani and 2.5% NaCl heart infusion (HI) media, respectively. Antibiotics were used as previously described (25).

Construction of deletion mutants and complementation. We constructed in-frame single, double, and triple deletion mutants of the entire structural genes in TonB1, TonB2, and TonB3 loci by the allelic-exchange method using the suicide vector pDM4 (26). For each TonB system, we designed two sets of primers to amplify DNA fragments in the upstream or downstream region of each operon. The sequences of each primer pair are listed in Table S1 in the supplemental material. Some primer sets included restriction site overhangs that were recognized by specific restriction enzymes for cloning. The upstream and downstream amplicons of each TonB operon were ligated by crossover PCR to produce a 2-kb fragment (27). The fusion fragments were digested with the appropriate enzymes and subcloned into pDM4 for the *tonB1*, *tonB2*, and *tonB3* mutants, yielding pCMM1509, pCMM1510, and pCMM1511, respectively. All of the resulting recombinant pDM4 plasmids were transferred into *V. vulnificus* CMCP6 by conjugation, and the single-deletion mutants (Δ*tonB1*, Δ*tonB2*, and Δ*tonB3* mutants) were selected as previously described (28). The *tonB12* and *tonB13* double mutants (Δ*tonB12* and Δ*tonB13* mutants) were constructed by transferring pCMM1509 into the Δ*tonB2* and Δ*tonB3* mutants, respectively. The *tonB23* double and *tonB123* triple mutants (Δ*tonB23* and Δ*tonB123* mutants) were constructed by transferring pCMM1511 into the Δ*tonB2* and Δ*tonB12* mutants, respectively. For genetic complementation experiments, we screened cosmid clones that contained an intact *tonB1*, *tonB2*, or *tonB3* operon from the pLAFR3 cosmid library of *V. vulnificus* CMCP6 as previously described (29), yielding pCMM1512 (*ptonB1*), pCMM1513 (*ptonB2*), and pCMM1514 (*ptonB3*), respectively. The positive colony was transferred to deletion mutants by triparental mating with the conjugative helper plasmid pRK2013. The transconjugants were selected as previously described (29).

Cytotoxicity assay. To determine the effect of TonB mutations on cytotoxicity for HeLa cells, we performed the lactate dehydrogenase (LDH) release assay as previously described (30).

LD_{50} determination. The intraperitoneal 50% lethal doses (i.p. LD_{50}) of *V. vulnificus* were determined using normal and iron-overloaded mice as previously described (30). Briefly, for the iron-overloading experiment, groups of 7-week-old randomly bred specific-pathogen-free (SPF) female CD-1 mice (Daehan Animal Co., Daejeon, South Korea) were i.p. injected with 900 μg of ferric ammonium citrate (filter sterilized; 100 μg of elemental iron) in phosphate-buffered saline (PBS) for 30 min before bacterial challenge. Five mice per group were administered 10-fold serial dilutions of fresh bacterial suspensions, and the infected mice were observed for 48 h. The intragastric 50% lethal dose (i.g. LD_{50}) was tested using randomly bred SPF CD-1 suckling mice (Daehan Animal Co., Daejeon, South Korea). Six-day-old infant mice were administered 10-fold serial dilutions of fresh bacterial suspensions containing 0.1% Evans blue (Sigma-Aldrich Co., St. Louis, MO) to ensure correct i.g. administration. The control animals received 100 μl of PBS containing 0.1% Evans blue. The challenged mice were monitored for 48 h. Seven mice per group were used

for analysis. LD_{50} was calculated by the probit analysis, using IBM SPSS 21.0 software (IBM). All of the animal procedures were conducted in accordance with the guidelines of the Animal Care and Use Committee of Chonnam National University, South Korea.

***In vivo* invasion assay.** The bacterial cells that translocated from the intestine to the bloodstream were measured as previously described (31, 32). Seven-week-old SPF female CD-1 mice were starved for 16 h and anesthetized with a mixture of 10% zolazepam-tiletamine (Zoletil; Virbac Laboratories, France) and 5% xylazine (Rumpun; Byer Korea, South Korea) dissolved in PBS. The ileum was tied off in a 5-cm segment, and then *V. vulnificus* cells (4.0×10^6 CFU/400 μl in PBS) were inoculated into the ligated segment. The blood samples were acquired by cardiac puncture at various time intervals. Viable bacterial cells were counted by plating on 2.5% NaCl HI agar plates. Remaining *V. vulnificus* cells in ligated ileal loops were also counted by plating on *Vibrio*-selective thiosulfate-citrate-bile salts-sucrose (TCBS) agar plates.

***In vitro* invasion assay.** Polarized HCA-7 cells grown on Transwell filter chambers (8-μm pore size; Costar, Cambridge, MA, USA) were apically exposed to log-phase *V. vulnificus* cells at a multiplicity of infection (MOI) of 5 under serum-free conditions. The invasiveness was determined by measuring the change in transepithelial electrical resistance (33) and the number of bacterial cells that translocated from the upper chamber to the lower chamber of the Transwell (32). Viable bacterial cells were counted by plating on 2.5% NaCl HI agar plates. LDH release from polarized HCA-7 cells was measured in culture media collected from the upper and lower chambers of the Transwells using the CytoTox nonradioactive cytotoxicity assay kit (Promega, Madison, WI, USA).

Growth of the bacteria in the rat peritoneal cavity and mouse blood. The *in vivo* growth of *V. vulnificus* was measured using a dialysis tube implantation model. CelluSep H1 dialysis tubing (molecular weight cutoff [MWCO], ~12,000 to 14,000; Membrane Filtration Products, Inc., TX, USA) was incubated with PBS overnight. The dialysis membrane was disinfected with 70% alcohol for 1 h and washed three times with sterile PBS before use. Seven-week-old female Sprague Dawley (SD) rats (DBL Co. Ltd., Daejeon, South Korea) were anesthetized with a mixture of 10% zolazepam-tiletamine and 5% xylazine dissolved in PBS. Three 10-cm dialysis tubes that contained 2 ml of 5×10^5 CFU/ml *V. vulnificus* cells were surgically implanted into the rat peritoneal cavity. The bacterial growth at each time point was analyzed using three rats. The bacteria were harvested for viable-cell counting on 2.5% NaCl HI agar plates after 2, 4, and 6 h of implantation.

For growth in blood, each mouse was intravenously injected with 100 μl of 5×10^5 CFU cells which had been incubated in the rat peritoneal cavity for 6 h for *in vivo* adaptation. After various times, blood samples were acquired from infected mice by cardiac puncture. Viable bacterial cells were counted by plating on 2.5% NaCl HI agar plates.

Host cell adhesion assay. For the adhesion assay, HeLa cell monolayers were seeded on chamber slides (Nunc) and then infected with log-phase *V. vulnificus* cells at an MOI of 250 for 30 min. The monolayer was then washed twice with PBS to remove nonadherent bacteria. Following the last wash, cells were fixed in methanol and stained with 0.1% Giemsa (Sigma). The *V. vulnificus* cells that adhered to HeLa cells were enumerated and examined under a light microscope at magnifications of ×400 and ×1,000 (Eclipse 50i; Nikon, Japan).

Motility assay. For motility assays, 1 μl of 1×10^9 CFU/ml log-phase *V. vulnificus* cells was inoculated on motility assay agar (0.3% agar–2.5% NaCl HI plate) and incubated at 37°C. Zones of migration were observed after 12 h.

Electron microscopy. *V. vulnificus* strains were grown to mid-log phase in 2.5% NaCl HI broth without agitation. The *V. vulnificus* cells were fixed in a fixation solution containing 0.1% glutaraldehyde and 4% paraformaldehyde in 0.05 M sodium cacodylate buffer (pH 7.2) at room temperature for 4 h. After three washes with 0.05 M cacodylate buffer, all samples were mounted on nickel grids coated with carbon film (150 mesh). After staining with 2% uranyl acetate, the samples were examined with a transmission electron microscope (JEM-1400; JEOL Ltd., Japan) at 80-kV acceleration. The morphological differences of bacterial strains were observed at a magnification of ×25,000.

Conventional and real-time RT-PCR. Transcription of the three structural *tonB* systems was determined by conventional and real-time RT-PCR. The 16S rRNA was used as the internal standard for conventional RT-PCR, and *gyrA* was chosen as a suitable reference gene for real-time RT-PCR, since the expression level was consistent under different experimental conditions (*in vivo* and *in vitro*), and it has amplification efficiencies comparable to those of the target *tonB* genes. Forward and reverse primer pairs were designed as shown in Table S2 in the supplemental material. The total RNA was isolated from log-phase bacterial cells that had been cultured in the rat peritoneal cavity or in 2.5% NaCl HI broth using an RNeasy minikit (Qiagen GmbH, Hilden, Germany). One microgram of purified RNA was converted to cDNA using the QuantiTect reverse transcription kit (Qiagen) according to the manufacturer's protocol, and 3 μg of RNA was used to evaluate *tonB3* expression. Real-time RT-PCR was performed to quantify each target transcript using the QuantiTect SYBR green PCR kit (Qiagen). The relative gene expression was normalized to the expression of *gyrA* (34) using the threshold cycle ($\Delta\Delta C_T$) method (35). Simultaneously, conventional RT-PCR was performed, and the amplicons were separated on 2% (wt/vol) agarose gels and stained with ethidium bromide. Additionally, transcription of *rtxA1* was also examined by conventional RT-PCR using the HeLa cell infection model. Log-phase *V. vulnificus* cells were exposed to HeLa cells for 30, 60, and 90 min. At various time points, the bacterial cells attached to the HeLa cells were scraped off, and total RNA was isolated as described above.

Western blot analysis. For RtxA1 detection, HeLa cells grown on 6-well plates were infected with *V. vulnificus* log-phase cells at an MOI of 100 under the serum-free conditions. After 30, 60, and 90 min of incubation, the bacterial cells attached to HeLa cells were lysed with lysis buffer (Cell Signaling) and concentrated with an Amicon Ultra-0.5 centrifugal filter (Merck KGaA, Darmstadt, Germany). The samples were subjected to 10% SDS-PAGE. The RtxA1 proteins were detected using an anti-C-terminal GD-rich domain (anti-GD domain) antibody (RtxA1-C, a band of approximately 130 kDa) (36). For the Western blot analysis of FlaB, bacteria were cultured in 2.5% NaCl HI to log-phase growth, and then FlaB proteins in the bacterial cell pellet or the culture supernatant were detected using an anti-FlaB antibody (a band of approximately 42 kDa) as described previously (32).

Outer membrane protein purification. Changes in the outer membrane protein (OMP) profile of the mutant were tested. OMPs were purified by a method reported elsewhere (37). The OMP preparations were analyzed by 12% SDS-PAGE. The OMP bands showing differential expression between the wild-type and mutant were further identified by matrix-assisted laser desorption ionization–time of flight (MALDI-TOF MS).

DNA alignment. A Fur box was identified first in *E. coli* as a 19-bp palindromic sequence accommodating a Fur dimer (38). This Fur-binding motif is strictly conserved in other bacteria, including *Vibrio cholerae*, *Yersinia pestis*, and *Salmonella enterica* serovar Typhimurium, based on motif alignments of 5′ untranslated regions (UTRs) of Fur-regulated genes (39–41). This allowed us to use the same profile for the recognition of Fur boxes in the promoter regions of flagellin genes (GATAATGATA ATCATTATC). Multiple DNA alignments were constructed using CLUSTALX (42).

Statistical analysis. The results are expressed as means and standard errors of the means (SEM) unless otherwise stated. Each experiment was repeated a minimum of three times, and the results from representative samples are shown. Statistical analyses were performed using Prism 5.00 for Windows (GraphPad Software, San Diego, CA). Multiple comparisons were performed using Student's *t* test and analysis of variance (ANOVA) followed by Bonferroni *post hoc* tests. *P* values of <0.05 were considered statistically significant.

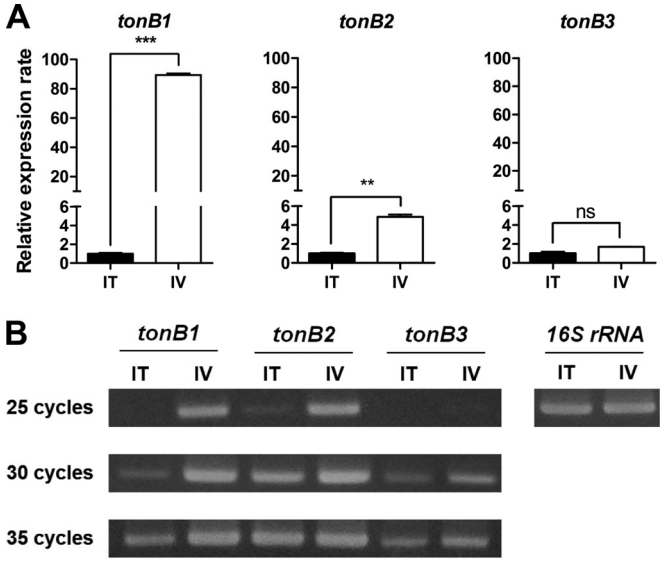

FIG 1 Transcription levels of the three structural *tonB* genes in *V. vulnificus* CMCP6. The transcription levels of the three structural *tonB* genes were analyzed by real-time (A) and conventional (B) RT-PCR under *in vitro* and *in vivo* conditions. RNA was isolated from the log-phase bacterial cells that had been cultured in the rat peritoneal cavity (*in vivo* [IV]) or in 2.5% NaCl HI broth (*in vitro* [IT]) and then converted to cDNA. qRT-PCR was performed, and the data were normalized to expression of the housekeeping gene *gyrA*. The values for the relative transcript abundance were expressed as mean-normalized gene expression relative to the *in vitro* expression values. The results showed that *tonB1* and *tonB2* genes are significantly induced *in vivo*, whereas *tonB3* is persistently transcribed at low levels under both tested conditions. The error bars represent the standard errors of means from three independent experiments. Statistical analysis was carried out using Student's *t* test (**, $P < 0.01$; ***, $P < 0.001$; ns, not significant).

RESULTS

The structural *tonB1* and *tonB2* genes are significantly induced *in vivo*, whereas *tonB3* is persistently transcribed at low levels under *in vitro* and *in vivo* conditions. Many important virulence genes of pathogenic bacteria are preferentially expressed *in vivo* (28, 43, 44). To see whether host signals could induce the transcription of three TonB systems of *V. vulnificus* CMCP6 during the infection process, we compared transcription levels of three structural *tonB* genes under *in vitro* and *in vivo* culture conditions by conventional and real-time RT-PCR (see Table S2 in the supplemental material). According to real-time RT-PCR results, higher levels of *tonB1* and *tonB2* mRNAs were observed under *in vivo* conditions than *in vitro* conditions, with approximately 90- and 5-fold changes, respectively (Fig. 1A) ($P < 0.001$ for *tonB1* and $P < 0.01$ for *tonB2*). Interestingly, low levels of transcripts of *tonB3* were obtained under both conditions using 3-fold more total RNA (3 μg) than for assessing *tonB1* and *tonB2* (1 μg). The comparable transcription levels of the *tonB3* gene by the real-time RT-PCR under both conditions indicated that this system would be persistently transcribed irrespective of the culture environment, albeit at a low expression level (Fig. 1A) ($P > 0.05$). The expression of three structural *tonB* genes was further confirmed through conventional RT-PCR with different amplification cycles. In agreement with the real-time PCR results, we detected significantly increased expression of *tonB1* and *tonB2* under *in vivo* conditions, whereas the expression of *tonB3* was detected only in late cycles under both conditions (Fig. 1B). These findings led us to hypothesize that all three TonB systems would be functional, which drove us to further investigate the role of three TonB systems in the pathogenesis of *V. vulnificus* CMCP6 infections.

Cytotoxicity was delayed only in the *tonB123* triple mutant and was significantly recovered by complementation with each TonB system. To evaluate the pathogenic significance of three TonB systems in *V. vulnificus*, in-frame single (Δ*tonB1*, Δ*tonB2*, and Δ*tonB3*), double (Δ*tonB12*, Δ*tonB13*, and Δ*tonB23*), and triple (Δ*tonB123*) deletion mutants were constructed (see Table S1 in the supplemental material). The cytotoxicity of *V. vulnificus* was measured in a time course. Interestingly, only the Δ*tonB123* mutant exhibited significantly delayed cytotoxicity, whereas the single and double mutants showed little or no changes during 3.5 h of the assay (Fig. 2A) ($P < 0.001$). The cytotoxicity of the Δ*tonB123* mutant approached the wild-type level after 3 h of in-

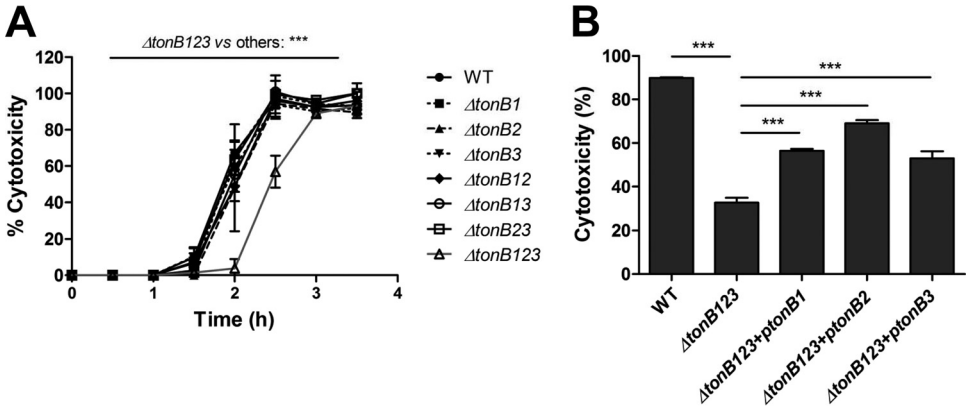

FIG 2 Significantly delayed cytotoxicity for HeLa cells in the *tonB123* triple mutant (A) and the complemented strain (B). (A) Log-phase *V. vulnificus* cells were incubated with HeLa cells at an MOI of 100. Statistical analysis of the *tonB123* mutant using two-way ANOVA followed by Bonferroni *post hoc* tests revealed significantly delayed cytotoxicity for HeLa cells in comparison with the wild type and other mutant strains (***, $P < 0.001$). (B) Restoration of the cytotoxicity in the TonB-complemented strains at 2.5 h. The values are means plus SEM from three independent experiments that were performed in six replicates. Comparisons were performed using one-way analysis of variance (ANOVA) followed by Bonferroni *post hoc* tests on the data in panel B (***, $P < 0.001$). WT, wild type.

TABLE 2 Effect of the mutation of all three TonB systems on the lethality to mice

Infection and mouse type	LD_{50} (95% confidence limits)		Fold increase
	WT	Δ*tonB123* mutant	
Intragastric			
Suckling	1.26×10^5 (2.16×10^4 to 4.82×10^5)	5.23×10^6 (3.32×10^5 to 9.95×10^7)	41.62
Intraperitoneal			
Normal	3.15×10^5 (8.38×10^4 to 1.13×10^6)	8.12×10^6 (2.04×10^6 to 3.1×10^7)	25.78
Iron overloaded	2.125	2.125	1

cubation (Fig. 2A). Full cytotoxic expression was delayed by 30 min in the Δ*tonB123* mutant compared to the wild-type strain.

In an attempt to fulfill the molecular Koch's postulates, we performed a complementation study. We first selected cosmid clones that contain an intact TonB1, TonB2, or TonB3 operon by screening of a pLAFR3 cosmid library of *V. vulnificus* CMCP6 as previously described (29). The Δ*tonB123* mutation was separately complemented with the individual cosmid clone harboring each TonB operon. The restoration of expression of each TonB operon was confirmed in the TonB-complemented strains by RT-PCR (see Fig. S1A in the supplemental material). The Δ*tonB123* mutant significantly recovered cytotoxicity when complemented with any one of the three TonB operons (Fig. 2B) ($P < 0.001$). Interestingly, complementation with the TonB2 operon restored most the cytotoxicity, while TonB1 and TonB3 complementation showed levels of cytotoxicity comparable to each other. This result suggests that the TonB2 system plays a dominant role as reported previously (20, 21) compared to the other two systems and that TonB3 is as efficient as the TonB1 in the complementation of the *tonB123* mutation. The cytotoxicity defect of the Δ*tonB123* mutant could have resulted from a possible bacterial growth retardation in the cell culture medium. To ascertain this possibility, we also checked growth profiles of *V. vulnificus* strains in high-glucose DMEM, which was used for cytotoxicity assays (see Fig. S2 in the supplemental material). The growth profile of the Δ*tonB123* mutant was identical to that of the wild-type strain, suggesting that the growth difference was not the cause of cytotoxicity impairment. Based upon these results, we hypothesized that another specific virulence factor(s) related to cytotoxicity was affected by the *tonB123* mutation.

All three TonB systems contribute to *V. vulnificus* lethality for mice. To examine the contribution of three TonB systems to the mouse lethality, the i.g. LD_{50} was measured using 6-day-old suckling mice. As shown in Table 2, a complete deficiency of TonB function (Δ*tonB123*) resulted in a 42-fold increase in the i.g. LD_{50} compared with that of the wild-type strain. Significantly prolonged survival was observed in the groups given the Δ*tonB123* strain at all infection dosages (see Fig. S3 in the supplemental material) ($P < 0.05$ at 10^9, 10^7, and 10^6 CFU/mouse, and $P < 0.01$ at 10^8 CFU/mouse, by Kaplan-Meier survival analysis). At doses of 10^9 CFU/mouse, all mice infected with the wild-type strain died, whereas only ca. 30% of infected mice died in the group receiving the Δ*tonB123* strain by 12 h postinfection (see Fig. S3 in the supplemental material) ($P < 0.05$, log rank test). Together, the results highlight the idea that all three TonB systems contribute to the *in vivo* virulence expression of *V. vulnificus* CMCP6.

In addition to the i.g. infection, we also measured the i.p. LD_{50} in normal and iron-overloaded mice. The i.p. LD_{50} of the Δ*tonB123* mutant increased 26-fold in normal mice, whereas no change was noted in iron-overloaded mice (Table 2). It was interesting that the lethality of the Δ*tonB123* mutant for mice was as strong as that of the parental wild-type strain in hosts having high levels of iron. These results imply that the three TonB systems play an important role in acquiring iron under iron-limited rather than iron-sufficient conditions. The difference in LD_{50} between the Δ*tonB123* and wild-type strains was smaller in the i.p. infection model (26-fold) than the i.g. infection model (42-fold). Since the i.g. infection route simulates more physiologically the primary *V. vulnificus* septicemia infection process in humans, the three TonB systems might significantly contribute to the virulence factor expression or survival of *V. vulnificus* CMCP6 during the early invasion phase of primary infection. In this context, we next tested the tissue invasiveness of the Δ*tonB123* mutant.

All three TonB systems contribute to the intestinal invasion of *V. vulnificus*. To corroborate whether the three TonB systems contribute to the invasiveness of *V. vulnificus* CMCP6, we performed an *in vivo* invasion assay using the mouse ligated-ileal-loop infection model (32). Viable *V. vulnificus* cells in the blood were counted at 3, 6, and 8 h to evaluate the tissue invasiveness of the Δ*tonB123* mutant. At 3 h, both strains were discovered in blood circulation at comparable numbers (Fig. 3A) ($P > 0.05$). Significantly higher numbers of wild-type cells were counted at later time points, approximately 1.3×10^6 and 3.0×10^6 CFU/ml of wild-type cells at 6 h and 8 h, respectively (Fig. 3A) ($P < 0.05$). During these experiments, we found that 40% of the infected wild-type mice succumbed to the infection when the cell counts reached approximately 1×10^7 CFU/ml of blood (data not shown). In contrast, the defects of the Δ*tonB123* mutant resulted in a significant decrease in the translocation of *V. vulnificus* from the intestinal tract into the bloodstream; only ca. 4.0×10^3 CFU/ml of the Δ*tonB123* cells were detected in the bloodstream even at 6 and 8 h (Fig. 3A) ($P < 0.05$ compared to that of the wild-type strain).

In parallel with viable cells in the blood, we also counted bacterial cells in the ileum at various time points. At 3 h, we also detected comparable numbers of *V. vulnificus* in the ileum in both strains (Fig. 3B) ($P > 0.05$). However, the viable-cell count of the Δ*tonB123* mutant was significantly higher than that of the wild-type strain at later time points (Fig. 3B) ($P < 0.01$ at 6 h and $P < 0.05$ at 8 h). The nonfunctional TonB systems in the Δ*tonB123* mutant seemed to have no influence on growth in the ileum, since the viable-cell count steadily increased up to 1.0×10^7 CFU/ml in a time course. To confirm further that the attenuated invasion property of the mutant was due to the growth retardation, we checked *in vivo* growth using the peritoneal dialysis tube implantation model and the growth in mouse blood. The growth profiles

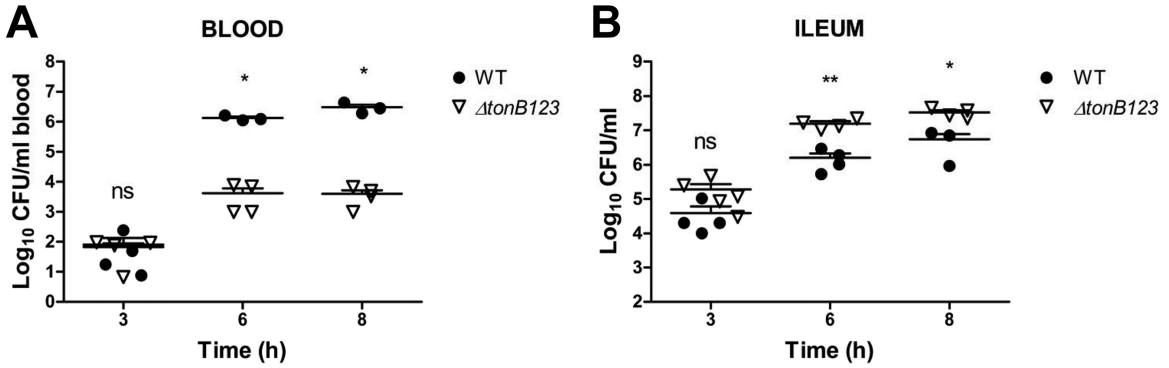

FIG 3 Impaired transepithelial invasion of the *tonB123* triple mutant. *V. vulnificus* (4.0×10^6 CFU/400 μl) was inoculated into ligated ileal loops of mice under anesthesia. (A) After the indicated times, blood samples were acquired from infected mice by cardiac puncture. Viable cells were counted by plating on 2.5% NaCl HI agar plates. (B) The remaining *V. vulnificus* cells in ligated ileal loops were also counted by plating on TCBS agar plates. The data are averages and SEM for at least three mice, and the experiment was repeated three times. Statistical analysis was carried out using Student's *t* test (*, $P < 0.05$, and **, $P < 0.01$, compared to the wild-type strain).

of the wild-type and the Δ*tonB123* mutant were identical in the dialysis tubes implanted in the rat peritoneum (see Fig. S4B [panel a] in the supplemental material). We also observed a similar pattern of viable-cell counts of both strains in the mouse blood, a rapidly decreasing curve over time, since viable bacteria were removed, presumably by a multitude of host defense mechanisms, such as complement-mediated lysis, phagocytosis, and antimicrobial peptide-mediated killing (see Fig. S4B [panel b] in the supplemental material). In this study, we could not observe significant differences in viable-cell counts in two different models, the culture in peritoneally implanted dialysis tubes filled with PBS (see Fig. S4B [panel a] in the supplemental material) and viable bacterial counting in the bloodstream (see Fig. S4B [panel b] in the supplemental material). Of note, the three TonB systems appeared to be dispensable for growth of *V. vulnificus* CMCP6 even in normal animals having intact iron-withholding ability. However, they appeared to play a significant role in providing invasive competence to *V. vulnificus* growing in the host environment. Taken together, these results support our hypothesis that the impaired transepithelial invasion of the Δ*tonB123* mutant is responsible for the incompetent intragastric infection by this strain.

A complete functional deficiency of *tonB123* significantly attenuated *in vitro* translocation across polarized intestinal epithelial monolayers. The invasiveness of *V. vulnificus* strains was further assessed using an *in vitro* intestinal epithelial barrier system. Polarized HCA-7 cells grown on Transwell filters were apically infected with *V. vulnificus* at an MOI of 5 under serum-free conditions. The change in transepithelial resistance (TER), which represents the tight junction disruption by bacterial infection, was measured. As shown in Fig. 4A, the TER gradually decreased after wild-type infection, whereas a significant delay was observed in HCA-7 cells infected with the Δ*tonB123* mutant for 6 h ($P < 0.001$). The invasiveness was quantified by measuring the number of bacterial cells that translocated from the upper to the lower chamber of the Transwell. Consistent with the *in vivo* data described above, approximately 3.8×10^5 CFU/ml of wild-type cells were detected in the lower chamber after 3 h of incubation, and the cell counts reached 5.0×10^8 CFU/ml after 6 h, whereas the translocation of the Δ*tonB123* mutant was not detected up to 5 h after infection (Fig. 4B) ($P < 0.001$). In parallel with the translocation of *V. vulnificus*, the LDH release in the lower chamber gradually increased and reached 100% by 6 h following wild-type infection, whereas negligible LDH release was detected from the Δ*tonB123* mutant-infected cells (Fig. 4C) ($P < 0.001$). The cytotoxicity to HCA-7 cells in the upper chamber was also delayed in the Δ*tonB123* strain, as observed with the HeLa cell infection model (Fig. 4D) ($P < 0.001$). The *in vitro* data, coupled with the *in vivo* invasion results, demonstrate the importance of three TonB systems for traversing the intestinal epithelial barrier by virulent *V. vulnificus* CMCP6.

All three TonB systems contribute to the motility and adhesion of *V. vulnificus* CMCP6. Based on the above results, we speculated that the defects of the Δ*tonB123* mutant somehow affected bacterial attachment to host cells, leading to defects in transepithelial invasion into the bloodstream or in translocation to the lower Transwell chamber. First, we performed the adhesion assay in which HeLa cells were infected with *V. vulnificus* strains at an MOI of 250, and the bacterial cells that adhered to host cells were counted. The number of the Δ*tonB123* cells that adhered to a single HeLa cell was approximately 34-fold lower than that of the wild-type strain after 30 min of infection (Fig. 5A) ($P < 0.001$). The wild-type strain formed small clusters of aggregated bacteria on the HeLa cell surface, consequently causing cell lysis. In contrast, few Δ*tonB123* cells attached to the HeLa cell surface, and the infected host cells maintained cell contours almost like those of uninfected cells (Fig. 5B, panel a). The adherence of the Δ*tonB123* mutant to host cells was further observed at later time points. The number of Δ*tonB123* cells adhering to HeLa cells gradually increased in a time-dependent manner (Fig. 5A and B, panel b), providing an explanation of why cytotoxicity was delayed in the Δ*tonB123* strain (Fig. 2A).

Given that motility is essential for the adhesion of enteropathogens to host cells (45), we further explored whether the Δ*tonB123* mutant also has a motility defect by measuring the migration of *V. vulnificus* on semisolid agar surfaces. The *tonB12* and *tonB123* mutants exhibited significant defects in motility compared with the wild-type strain (Fig. 6; also, see Fig. S5 in the supplemental material) ($P < 0.001$). Remarkably, the Δ*tonB123* mutant manifested a profound defect in motility relative to the Δ*tonB12* strain, showing an approximately 60% decrease in the migration area compared to a 10% decrease shown by the Δ*tonB12* strain (Fig. 6) ($P < 0.001$). The reduced motility in the Δ*tonB12* strain was fully

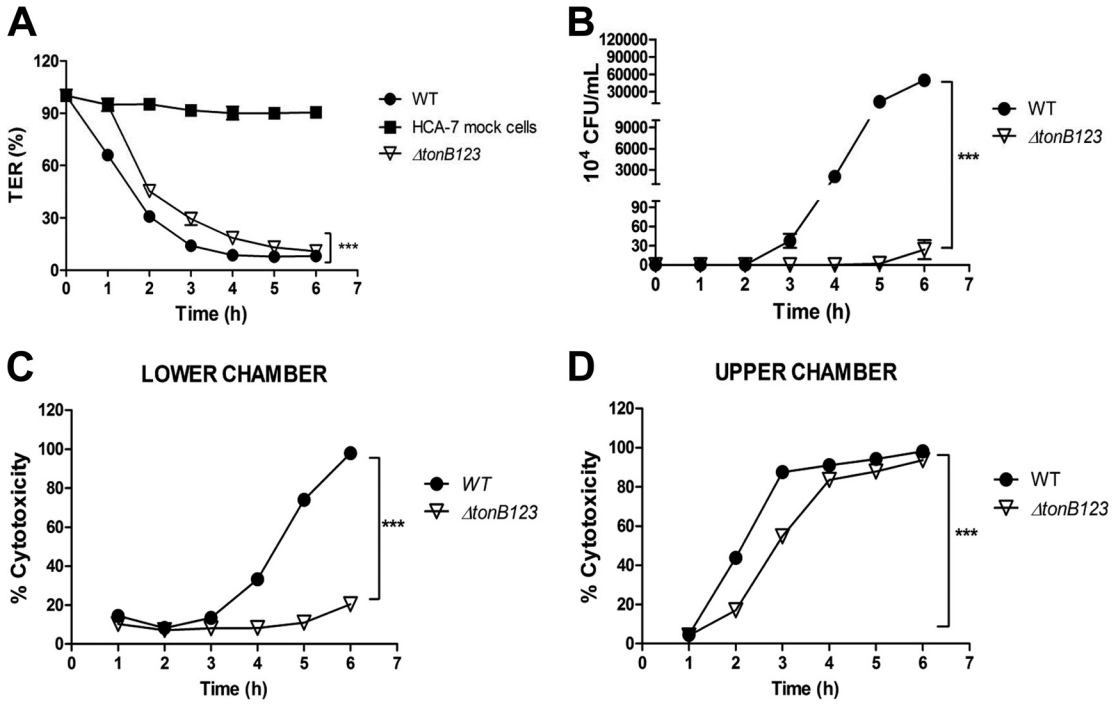

FIG 4 Attenuated translocation across a polarized HCA-7 monolayer in the *tonB123* triple mutant. HCA-7 cells grown on Transwell filters were apically exposed to log-phase *V. vulnificus* cells. The invasiveness was determined by measuring the change in TER (A) and the number of bacterial cells that translocated from the upper chamber to the lower chamber of the Transwell (B). Viable bacterial cells were counted by plating on 2.5% NaCl HI agar plates. The LDH release in the lower chamber (basolateral) (C) and the upper chamber (apical) (D) was also determined. The values are means and standard errors from three independent experiments that were performed in five replicates. Statistical analyses of the *tonB123* mutant using a two-way ANOVA followed by Bonferroni *post hoc* tests revealed an attenuated translocation across the polarized HCA-7 monolayer in the Δ*tonB123* mutant compared to the wild-type strain (***, $P < 0.001$).

restored by in *trans* complementation with any one of the three TonB systems (see Fig. S5B in the supplemental material), while the defect in the Δ*tonB123* mutant was not restore by any means (see Fig. S5C in the supplemental material). Taking these results together, we supposed that the defects of the Δ*tonB123* mutant in cytotoxicity and invasiveness could be attributed to the motility defect, which consequently resulted in decreased adhesion to host cells. The motility assay results once again indicated the dominant

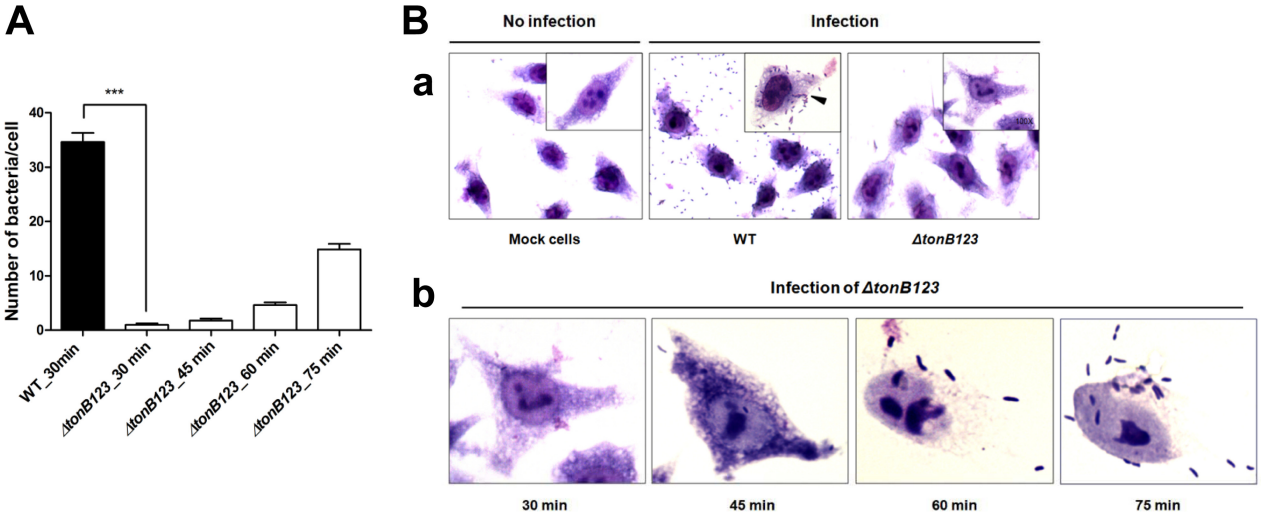

FIG 5 Significantly decreased adhesion to host cells in the *tonB123* triple mutant. (A) HeLa cells were treated with log-phase *V. vulnificus* cells at an MOI of 250 for 30, 45, 60, and 75 min, and the bacterial cells that adhered to the HeLa cells were counted. Data are means plus SEM from three independent experiments that were performed in 10 replicates. Statistical analysis was carried out using Student's *t* test (***, $P < 0.001$ compared to the wild-type strain). (B) Morphology of infected HeLa cells after Giemsa staining. (a) *V. vulnificus*-infected cells were observed after 30 min of infection (at magnifications of ×400 and ×1,000 [inset]). (b) The number of Δ*tonB123* cells adhering to HeLa cells gradually increased in a time-dependent manner (magnification, ×1,000). The adherent *V. vulnificus* cells (filled arrowhead) are indicated.

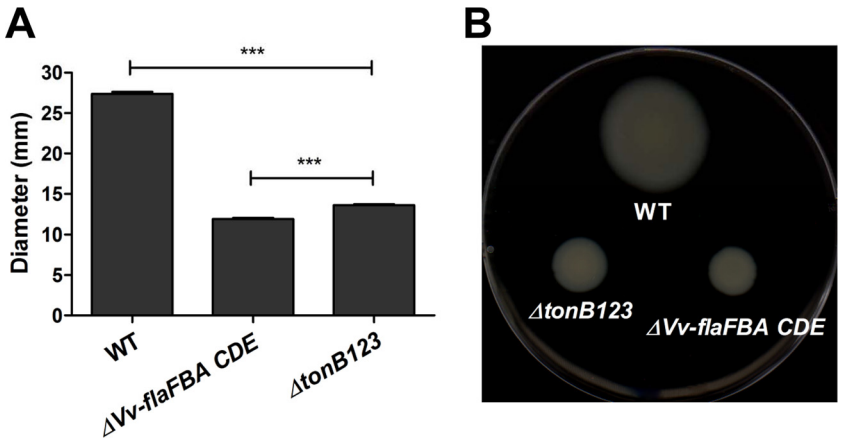

FIG 6 Decreased motility in the *tonB123* triple mutant. (A) Log-phase cells were inoculated onto motility agar plates containing 0.3% agar and incubated for 12 h at 37°C. The diameters of motility areas are the means plus SEM from three independent experiments that were performed in fifteen replicates. Statistical analysis was carried out using Student's *t* test (***, $P < 0.001$ compared to the wild-type strain). (B) The areas of motility of *V. vulnificus* were photographed.

functions of TonB1 and TonB2 reported previously by other groups (20, 21); the Δ*tonB12* mutant showed a significant motility defect, while all other single or double operon mutants did not show any change in motility. Next we tried to determine why motility was defective in the Δ*tonB123* mutant.

A complete functional deficiency of *tonB123* resulted in a significant decrease in the flagellin expression of *V. vulnificus* CMCP6. Previously, Alice et al. reported that the genes coding for flagellar proteins are induced under iron-rich conditions (20). It has been reported that flagellar biogenesis is a requisite for host cell adhesion and cytotoxicity (32, 45, 46). Hence, we speculated that the three TonB systems would play important roles in the flagellar biogenesis by supplying sufficient level of iron. In addition, we found the Fur-binding site (CAAATGATAATAATTTGC AAT) in the promoter regions of flagellin genes (see Table S3 in the supplemental material), strongly suggesting the relationship between TonB system-mediated iron assimilation and flagellation. We examined the transcription and translation of the flagellin genes in the wild-type and the Δ*tonB123* backgrounds. The transcripts of flagellin genes were determined by conventional and real-time RT-PCR (Fig. 7A). Since *V. vulnificus* CMCP6 has a total of six flagellin genes (*flaA*, *flaB*, *flaC*, *flaD*, *flaE*, and *flaF*) organized into two loci (*flaFBA* and *flaCDE*) in chromosome I (32), we designed two primer sets to amplify *flaF* and *flaC* for each flagellin cluster specifically. The amount of *flaF* and *flaC* amplicons in the Δ*tonB123* mutant was significantly lower than that in the wild-type strain (Fig. 7A) ($P < 0.001$ for *flaF* and $P < 0.01$ for *flaC*). Complementation with any TonB system could not restore flagellin gene expression in the Δ*tonB123* mutant (see Fig. S6 in the supplemental material) ($P > 0.05$). This result explained why complementation did not work for the motility of the Δ*tonB123* mutant, even with the dominant TonB2 operon (see Fig. S5C in the supplemental material).

To confirm the flagellin expression defect at the protein level, Western blot analysis was subsequently carried out in the *V. vulnificus* cell pellet and supernatant to detect FlaB, which has been well characterized as the representative and major flagellin structural protein among proteins with six flagellins (hexa flagellin proteins) (32). We observed a tight correlation between the quantitative RT-PCR (qRT-PCR) and Western blotting results. FlaB protein was detected in wild-type strain but not in the Δ*tonB123* mutant in both cell pellets and culture supernatants (Fig. 7B, panel a). Interestingly, the data were strongly supported by the changes in OMP profile of the *tonB123* mutant compared to the wild-type strain. Two major OMP bands were missing in the Δ*tonB123* strain which were subsequently identified as flagellin proteins (42 kDa) using MALDI-TOF MS (Fig. 7B, panel b). Additionally, electron microscopy showed that the Δ*tonB123* strain totally lacked flagellation, like the *flaFBA flaCDE* hexa mutant constructed in our previous study (32) (Fig. 7C). Taken together, the three TonB systems appear to play an essential role in the flagellation of *V. vulnificus* CMCP6 by supplying sufficient iron for the expression of flagellin genes.

The *tonB123* triple mutant was defective in the production of RtxA1 cytotoxin. RtxA1 is a crucial cytotoxin that is involved in cellular damage and the necrosis of infected tissues, allowing bacterial penetration into the bloodstream through the intestinal epithelium (31, 47–50). Previously, we reported that *V. vulnificus* CMCP6 induces RtxA1 toxin production to kill host cells after coming into close contact with host cells (31). We hypothesized that impaired attachment to host cells hampered production and consequently host cell killing and tissue invasion. We performed a Western blot analysis of cell pellets to assess toxin production at 30, 60, and 90 min after HeLa cell infection. RtxA1 was detected using an anti-GD domain antibody targeting the C-terminal fragment (RtxA1-C; approximately 130 kDa), which is internalized in the host cell cytoplasm (36). Significantly less RtxA1 protein was detected in the infection caused by the Δ*tonB123* mutant than in that caused by the wild-type strain (Fig. 8A). We also examined *rtxA1* transcription by RT-PCR using mRNA from bacterial cells that adhered to HeLa cells at various time points. Like the Western blot analysis, in the HeLa cell coculture model, the Δ*tonB123* mutant showed significantly less transcription of *rtxA1* at all time points tested than the wild-type strain (Fig. 8B), while a comparable transcription rate was observed in both strains in 2.5% NaCl HI broth (see Fig. S7 in the supplemental material). Thus, because of the difficulty of coming into contact with host cells (Fig. 5), the triple *tonB123* mutant manifested defective RtxA1 toxin production. The RtxA1 production in the Δ*tonB123* mutant was gradually delayed in a time-dependent manner (Fig. 8), which corre-

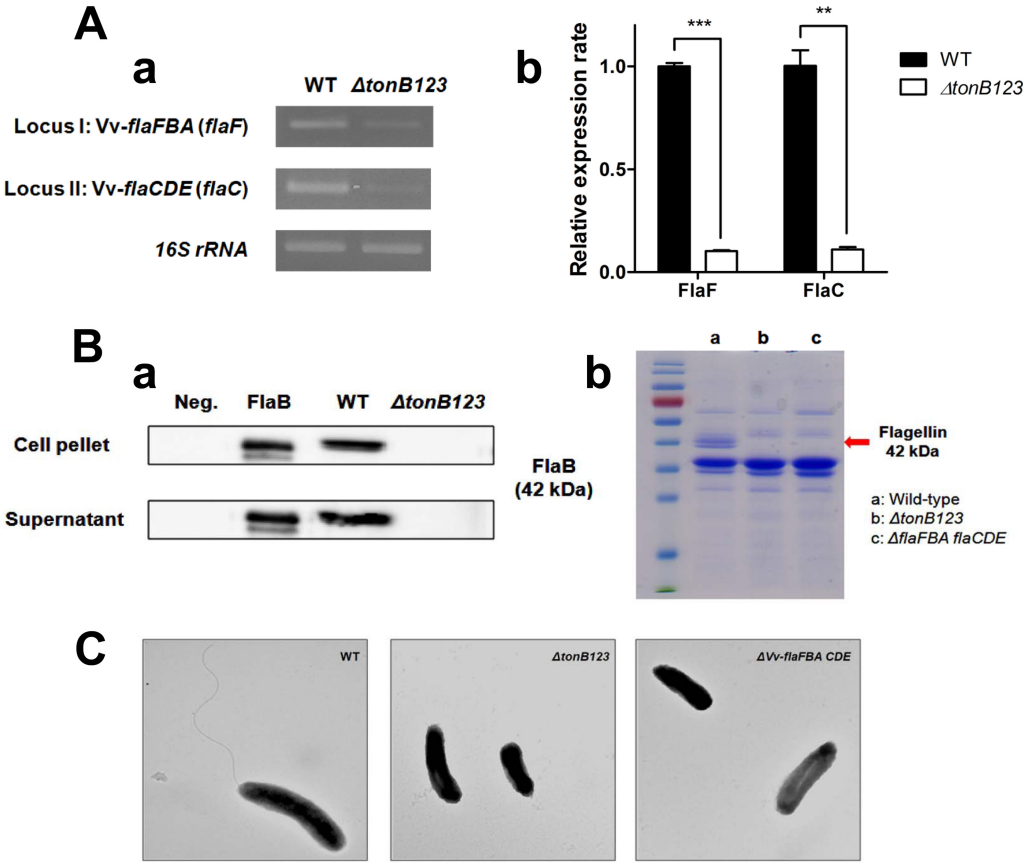

FIG 7 Defects of the transcription (A) and translation (B) of flagellin genes and loss of flagellation in the *tonB123* triple mutant (C). (A) RNA was isolated from log-phase bacterial cells that had been cultured in the rat peritoneal cavity and was then converted to cDNA. Conventional (a) and real-time (b) RT-PCR was performed using primers specific for *flaF* and *flaC*, as shown in Table S2 in the supplemental material. The error bars represent the standard errors of means from three independent experiments. Statistical analysis was carried out using Student's *t* test (**, $P < 0.01$, and ***, $P < 0.001$, compared to the wild-type strain). (B) (a) Bacteria were cultured in 2.5% NaCl HI to log-phase growth, and then Western blot analysis was subsequently carried out in the *V. vulnificus* cell pellet and culture supernatant using an anti-FlaB antibody (a band of approximately 42 kDa). The Δ*flaFBA flaCDE* strain was used as a negative control (Neg.). (b) The OMP preparations were analyzed by 12% SDS-PAGE. Two major OMP bands were missing in the Δ*tonB123* mutant compared to the wild-type strain, which were subsequently identified as flagellin proteins (42 kDa) using MALDI-TOF MS. (C) Electron micrograph of the log-phase *V. vulnificus* strains under ×25,000 magnification.

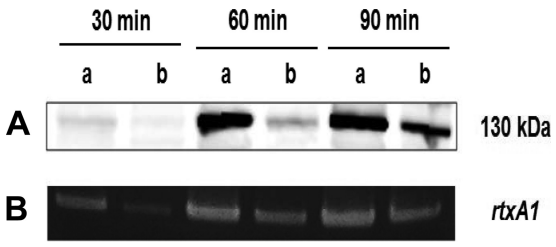

FIG 8 Significantly lower translation (A) and transcription (B) of *rtxA1* in the *tonB123* triple mutant infecting HeLa cells. (A) Log-phase *V. vulnificus* cells were incubated with HeLa cells on a 6-well plate at an MOI of 100 for 30, 60, and 90 min. The cells in each well were lysed by lysis buffer and concentrated with an Amicon Ultra-0.5 centrifugal filter. The RtxA1 proteins were detected by Western blotting using an anti-GD domain antibody (RtxA1-C, a band of approximately 130 kDa). (B) RNA was isolated from bacterial cells using a HeLa cell coculture model as described above. cDNA synthesis and RT-PCR were performed using primers specific for the *rtxA1* gene as shown in Table S2 in the supplemental material. Lanes: a, wild type; b, Δ*tonB123* mutant.

lated with host cell adhesion (Fig. 5) and cytotoxicity (Fig. 2A). The TonB systems seem to have no direct regulatory role with regard to the RtxA1 operon through Fur, since no conserved Fur-binding sites were found in the promoter region and the toxin production reached the wild-type level after a delayed attachment to host cells.

DISCUSSION

During the host-pathogen interaction, *V. vulnificus* is confronted with a host defense called "nutritional immunity" that sequesters essential nutrient metals, such as iron, which is required for heme biogenesis (51–55). Bacterial pathogens have developed a large variety of systems to take up those nutrients from animal hosts (4, 51). In Gram-negative bacteria, the TonB system plays crucial roles in the transport of iron-siderophore complexes (15, 16), vitamin B_{12} (14), and a wide range of substrates, including zinc, nickel, maltodextrins, and sucrose (17–19, 56). There are three TonB systems in *V. vulnificus* CMCP6 (20): TonB1 and TonB2 were reported to play predominant roles in the iron transport of siderophores and in the pathogenesis of *V. vulnificus* (20, 21),

while there is scanty functional information about TonB3. The maintenance of a third TonB system in *V. vulnificus* CMCP6 genomes, which is similar to the TonB2 system in its gene arrangement and orientation (20–22), raised the following questions. Why has *V. vulnificus* CMCP6 maintained three TonB systems throughout evolution? How does each TonB system contribute to the virulence of *V. vulnificus*, and are all three TonB systems necessary for the virulence? Through *in vitro* and *in vivo* experiments, in the present study we have addressed these questions, at least in part, and found that these systems are coordinated to contribute to *V. vulnificus* CMCP6 virulence. We demonstrated the contribution of three TonB systems to flagellation, motility, adhesion, cytotoxicity, invasion, and *in vivo* virulence. The three TonB systems appear to complement each other's functions, and only the complete abrogation of all three TonB operons caused severe defects in virulence phenotypes. This is the first report to document the association between TonB systems and flagellation in *V. vulnificus* CMCP6. Since proper flagellation is very important for flagellum-mediated locomotion in the marine environment and motility and adhesion to the host cells during infection (32, 45, 57), the pathogens that lost flagellation became impaired for contacting to host cells, leading to a decrease in RtxA1 production. As a result, a series of virulence defects were detected in the *tonB123* triple mutant, including delayed cytotoxicity, impaired invasiveness, and decreased lethality for mice.

In a previous study (20), Crosa's group showed that a mutant having in-frame deletions in both *tonB1* and *tonB2* genes (not all structural genes in TonB12 loci) manifested a 4-log scale increase of subcutaneous LD_{50} in iron-overloaded mice compared with the isogenic wild-type strain. Strangely, intraperitoneal infection did not show any LD_{50} difference between the mutant and wild-type strains in either iron-overloaded or normal-iron-level mice. The finding that only subcutaneous infection, not intraperitoneal infection, showed a significant virulence decrease in the mutant with defects in the TonB1 and TonB2 systems corroborates our suggestion: the TonB systems play important roles in the invasion process. However, their results are contradictory to ours in that we saw LD_{50} changes only in normal-iron-level mice, not in iron-overloaded mice. Given that TonB1 and TonB2 systems are induced by iron deprivation and play important roles in iron assimilation (20), it is curious that they observed virulence impairment only in iron-overloaded animals. As for experimental models, the only difference between our study and theirs is that we used deletions of the entire structural genes in TonB loci for functional inactivation, while they used in-frame deletions of the most important structural *tonB* genes in the operons. We cautiously speculate that our approach, using a complete functional deficiency of TonB systems and complementation with cosmid clones harboring whole operons, represents a broader range of physiological interaction landscapes among the three TonB systems in *V. vulnificus* CMCP6.

Taken together, the results reported here indicate that all three TonB systems of *V. vulnificus* CMCP6 coordinately complement each other for iron assimilation and full virulence expression by ensuring flagellar biogenesis. The major function of TonB systems might not be to supply iron for the *in vivo* growth of *V. vulnificus* CMCP6, since the *tonB123* triple mutant grew very well, like the isogenic wild-type strain, in the ileum (Fig. 3), in DMEM without iron supplementation (see Fig. S2 in the supplemental material), in the peritoneal cavity of normal rats (see Fig. S4B [panel a] in the supplemental material), and even in blood (see Fig. S4B [panel b] in the supplemental material). Rather, the raison d'être of three TonB systems in *V. vulnificus* CMCP6 should involve in supplying a sufficient level of iron, allowing the expression of flagellar biogenesis genes, which are located higher in the hierarchy of the virulence expression cascade. This hypothesis is corroborated by the report by Crosa's group showing that flagellar motility genes are induced under conditions of sufficient iron (20). Our new findings bring more critical insight into the pathogenic significance of these TonB systems in *V. vulnificus* CMCP6 and further suggest that new antibacterial agents that block the dual functions of TonB would suppress robust iron acquisition and virulence expression.

ACKNOWLEDGMENTS

This study was supported by a grant from the Korea Health Technology R&D Project through the KHIDI, funded by the MHW, Republic of Korea (HI14C0187), and an NRF grant from the MSIP (NRF-2013R1A2A2A01005011), Republic of Korea.

No potential conflicts of interest were disclosed.

FUNDING INFORMATION

MSIP, Republic of Korea provided funding to Shee Eun Lee under grant number NRF-2013R1A2A2A01005011. MHW, Republic of Korea provided funding to Joon Haeng Rhee under grant number HI14C0187.

REFERENCES

1. **Brennt CE, Wright AC, Dutta SK, Morris JG.** 1991. Growth of *Vibrio vulnificus* in serum from alcoholics: association with high transferrin iron saturation. J Infect Dis **164:**1030–1032. http://dx.doi.org/10.1093/infdis/164.5.1030.
2. **Ganz T, Nemeth E.** 2011. Hepcidin and disorders of iron metabolism. Annu Rev Med **62:**347–360. http://dx.doi.org/10.1146/annurev-med-050109-142444.
3. **Jones MK, Oliver JD.** 2009. *Vibrio vulnificus*: disease and pathogenesis. Infect Immun **77:**1723–1733. http://dx.doi.org/10.1128/IAI.01046-08.
4. **Linkous DA, Oliver JD.** 1999. Pathogenesis of *Vibrio vulnificus*. FEMS Microbiol Lett **174:**207–214. http://dx.doi.org/10.1111/j.1574-6968.1999.tb13570.x.
5. **Oliver JD.** 2005. Wound infections caused by *Vibrio vulnificus* and other marine bacteria. Epidemiol Infect **133:**383–391. http://dx.doi.org/10.1017/S0950268805003894.
6. **Strom MS, Paranjpye RN.** 2000. Epidemiology and pathogenesis of *Vibrio vulnificus*. Microbes Infect **2:**177–188. http://dx.doi.org/10.1016/S1286-4579(00)00270-7.
7. **Gulig PA BK, Starks AM.** 2005. Molecular pathogenesis of *Vibrio vulnificus*. J Microbiol **43:**118–131.
8. **Braun V.** 1995. Energy-coupled transport and signal transduction through the Gram-negative outer membrane via TonB-ExbB-ExbD-dependent receptor proteins. FEMS Microbiol Rev **16:**295–307. http://dx.doi.org/10.1111/j.1574-6976.1995.tb00177.x.
9. **Faraldo-Gomez JD, Sansom MSP.** 2003. Acquisition of siderophores in Gram-negative bacteria. Nat Rev Mol Cell Biol **4:**105–116. http://dx.doi.org/10.1038/nrm1015.
10. **Kim CM, Chung YY, Shin SH.** 2009. Iron differentially regulates gene expression and extracellular secretion of *Vibrio vulnificus* cytolysin-hemolysin. J Infect Dis **200:**582–589. http://dx.doi.org/10.1086/600869.
11. **Kim CM, Kim SC, Shin SH.** 2012. Iron-mediated regulation of metalloprotease VvpE production in *Vibrio vulnificus*. New Microbiol **35:**481–486.
12. **Wright AC, Simpson LM, Oliver JD.** 1981. Role of iron in the pathogenesis of *Vibrio vulnificus* infections. Infect Immun **34:**503–507.
13. **Larsen RA, Letain TE, Postle K.** 2003. *In vivo* evidence of TonB shuttling between the cytoplasmic and outer membrane in *Escherichia coli*. Mol Microbiol **49:**211–218. http://dx.doi.org/10.1046/j.1365-2958.2003.03579.x.
14. **Shultis DD, Purdy MD, Banchs CN, Wiener MC.** 2006. Outer membrane active transport: structure of the BtuB:TonB complex. Science **312:**1396–1399. http://dx.doi.org/10.1126/science.1127694.
15. **Miethke M, Marahiel MA.** 2007. Siderophore-based iron acquisition and

pathogen control. Microbiol Mol Biol Rev **71:**413–451. http://dx.doi.org/10.1128/MMBR.00012-07.
16. **Wandersman C, Delepelaire P.** 2004. Bacterial iron sources: from siderophores to hemophores. Annu Rev Microbiol **58:**611–647. http://dx.doi.org/10.1146/annurev.micro.58.030603.123811.
17. **Blanvillain S, Meyer D, Boulanger A, Lautier M, Guynet C, Denancé N, Vasse J, Lauber E, Arlat M.** 2007. Plant carbohydrate scavenging through tonB-dependent receptors: a feature shared by phytopathogenic and aquatic bacteria. PLoS One **2:**e224. http://dx.doi.org/10.1371/journal.pone.0000224.
18. **Neugebauer H, Herrmann C, Kammer W, Schwarz G, Nordheim A, Braun V.** 2005. ExbBD-dependent transport of maltodextrins through the novel MalA protein across the outer membrane of *Caulobacter crescentus*. J Bacteriol **187:**8300–8311. http://dx.doi.org/10.1128/JB.187.24.8300-8311.2005.
19. **Schauer K, Gouget B, Carrière M, Labigne A, De Reuse H.** 2007. Novel nickel transport mechanism across the bacterial outer membrane energized by the TonB/ExbB/ExbD machinery. Mol Microbiol **63:**1054–1068. http://dx.doi.org/10.1111/j.1365-2958.2006.05578.x.
20. **Alice AF, Naka H, Crosa JH.** 2008. Global gene expression as a function of the iron status of the bacterial cell: influence of differentially expressed genes in the virulence of the human pathogen *Vibrio vulnificus*. Infect Immun **76:**4019–4037. http://dx.doi.org/10.1128/IAI.00208-08.
21. **Kustusch RJ, Kuehl CJ, Crosa JH.** 2012. The *ttpC* gene is contained in two of three TonB systems in the human pathogen *Vibrio vulnificus*, but only one is active in iron transport and virulence. J Bacteriol **194:**3250–3259. http://dx.doi.org/10.1128/JB.00155-12.
22. **Alice AF, Crosa JH.** 2012. The TonB3 system in the human pathogen *Vibrio vulnificus* is under the control of the global regulators Lrp and cyclic AMP receptor protein. J Bacteriol **194:**1897–1911. http://dx.doi.org/10.1128/JB.06614-11.
23. **Kim HU, Kim SY, Jeong H, Kim TY, Kim JJ, Choy HE, Yi KY, Rhee JH, Lee SY.** 2011. Integrative genome-scale metabolic analysis of *Vibrio vulnificus* for drug targeting and discovery. Mol Syst Biol **7:**460–460. http://dx.doi.org/10.1038/msb.2010.115.
24. **Morrison SS, Williams T, Cain A, Froelich B, Taylor C, Baker-Austin C, Verner-Jeffreys D, Hartnell R, Oliver JD, Gibas CJ.** 2012. Pyrosequencing-based comparative genome analysis of *Vibrio vulnificus* environmental isolates. PLoS One **7:**e37553. http://dx.doi.org/10.1371/journal.pone.0037553.
25. **Tan W, Verma V, Jeong K, Kim SY, Jung CH, Lee SE, Rhee JH.** 2014. Molecular characterization of vulnibactin biosynthesis in *Vibrio vulnificus* indicates the existence of an alternative siderophore. Front Microbiol **5:**1.
26. **Miller VL, Mekalanos JJ.** 1988. A novel suicide vector and its use in construction of insertion mutations: osmoregulation of outer membrane proteins and virulence determinants in *Vibrio cholerae* requires *toxR*. J Bacteriol **170:**2575–2583.
27. **Horton RM, Hunt HD, Ho SN, Pullen JK, Pease LR.** 1989. Engineering hybrid genes without the use of restriction enzymes: gene splicing by overlap extension. Gene **77:**61–68. http://dx.doi.org/10.1016/0378-1119(89)90359-4.
28. **Kim YR, Lee SE, Kim CM, Kim SY, Shin EK, Shin DH, Chung SS, Choy HE, Progulske-Fox A, Hillman JD, Handfield M, Rhee JH.** 2003. Characterization and pathogenic significance of *Vibrio vulnificus* antigens preferentially expressed in septicemic patients. Infect Immun **71:**5461–5471. http://dx.doi.org/10.1128/IAI.71.10.5461-5471.2003.
29. **Kim SY, Lee SE, Kim YR, Kim CM, Ryu PY, Choy HE, Chung SS, Rhee JH.** 2003. Regulation of *Vibrio vulnificus* virulence by the LuxS quorum-sensing system. Mol Microbiol **48:**1647–1664. http://dx.doi.org/10.1046/j.1365-2958.2003.03536.x.
30. **Lee SE, Kim SY, Kim CM, Kim MK, Kim YR, Jeong K, Ryu HJ, Lee YS, Chung SS, Choy HE, Rhee JH.** 2007. The *pyrH* gene of *Vibrio vulnificus* is an essential *in vivo* survival factor. Infect Immun **75:**2795–2801. http://dx.doi.org/10.1128/IAI.01499-06.
31. **Kim YR, Lee SE, Kook H, Yeom JA, Na HS, Kim SY, Chung SS, Choy HE, Rhee JH.** 2008. *Vibrio vulnificus* RTX toxin kills host cells only after contact of the bacteria with host cells. Cell Microbiol **10:**848–862. http://dx.doi.org/10.1111/j.1462-5822.2007.01088.x.
32. **Kim SY, Thanh XTT, Jeong K, Kim SB, Pan SO, Jung CH, Hong SH, Lee SE, Rhee JH.** 2014. Contribution of six flagellin genes to the flagellum biogenesis of *Vibrio vulnificus* and *in vivo* invasion. Infect Immun **82:**29–42. http://dx.doi.org/10.1128/IAI.00654-13.
33. **Lee J, Mo JH, Katakura K, Alkalay I, Rucker AN, Liu YT, Lee HK, Shen C, Cojocaru G, Shenouda S, Kagnoff M, Eckmann L, Ben-Neriah Y, Raz E.** 2006. Maintenance of colonic homeostasis by distinctive apical TLR9 signalling in intestinal epithelial cells. Nat Cell Biol **8:**1327–1336. http://dx.doi.org/10.1038/ncb1500.
34. **Lo Scrudato M, Blokesch M.** 2012. The regulatory network of natural competence and transformation of *Vibrio cholerae*. PLoS Genet **8:**e1002778. http://dx.doi.org/10.1371/journal.pgen.1002778.
35. **Livak KJ, Schmittgen TD.** 2001. Analysis of relative gene expression data using real-time quantitative PCR and the 2-ΔΔCT method. Methods **25:**402–408. http://dx.doi.org/10.1006/meth.2001.1262.
36. **Kim YR, Lee SE, Kang IC, Nam KI, Choy HE, Rhee JH.** 2013. A bacterial RTX toxin causes programmed necrotic cell death through calcium-mediated mitochondrial dysfunction. J Infect Dis **207:**1406–1415. http://dx.doi.org/10.1093/infdis/jis746.
37. **Lee SE, Shin SH, Kim SY, Kim YR, Shin DH, Chung SS, Lee ZH, Lee JY, Jeong KC, Choi SH, Rhee JH.** 2000. *Vibrio vulnificus* has the transmembrane transcription activator ToxRS stimulating the expression of the hemolysin gene *vvhA*. J Bacteriol **182:**3405–3415. http://dx.doi.org/10.1128/JB.182.12.3405-3415.2000.
38. **Ptashne M.** 1992. A genetic switch: phage λ and higher organisms, 2nd ed. Cell Press & Blackwell Scientific Publications, Cambridge, MA.
39. **Tsolis RM, Bäumler AJ, Stojiljkovic I, Heffron F.** 1995. Fur regulon of *Salmonella typhimurium*: identification of new iron-regulated genes. J Bacteriol **177:**4628–4637.
40. **Goldberg MB, Boyko SA, Calderwood SB.** 1990. Transcriptional regulation by iron of a *Vibrio cholerae* virulence gene and homology of the gene to the *Escherichia coli* Fur system. J Bacteriol **172:**6863–6870.
41. **Gao H, Zhou D, Li Y, Guo Z, Han Y, Song Y, Zhai J, Du Z, Wang X, Lu J, Yang R.** 2008. The iron-responsive Fur regulon in *Yersinia pestis*. J Bacteriol **190:**3063–3075. http://dx.doi.org/10.1128/JB.01910-07.
42. **Thompson JD, Gibson TJ, Plewniak F, Jeanmougin F, Higgins DG.** 1997. The CLUSTAL_X Windows interface: flexible strategies for multiple sequence alignment aided by quality analysis tools. Nucleic Acids Res **25:**4876–4882. http://dx.doi.org/10.1093/nar/25.24.4876.
43. **Heithoff DM, Conner CP, Mahan MJ.** 1997. Dissecting the biology of a pathogen during infection. Trends Microbiol **5:**509–513. http://dx.doi.org/10.1016/S0966-842X(97)01153-0.
44. **Lee SH, Hava DL, Waldor MK, Camilli A.** 1999. Regulation and temporal expression patterns of Vibrio cholerae virulence genes during Infection. Cell **99:**625–634. http://dx.doi.org/10.1016/S0092-8674(00)81551-2.
45. **Lee JH, Rho JB, Park KJ, Kim CB, Han YS, Choi SH, Lee KH, Park SJ.** 2004. Role of flagellum and motility in pathogenesis of *Vibrio vulnificus*. Infect Immun **72:**4905–4910. http://dx.doi.org/10.1128/IAI.72.8.4905-4910.2004.
46. **Terashima H, Kojima S, Homma M.** 2008. Flagellar motility in bacteria: structure and function of flagellar motor. Int Rev Cell Mol Biol **270:**39–85. http://dx.doi.org/10.1016/S1937-6448(08)01402-0.
47. **Hor LI, Chen CL.** 2013. Cytotoxins of *Vibrio vulnificus*: functions and roles in pathogenesis. BioMedicine **3:**19–26. http://dx.doi.org/10.1016/j.biomed.2012.12.003.
48. **Jeong HG, Satchell KJ.** 2012. Additive function of *Vibrio vulnificus* MARTX(Vv) and VvhA cytolysins promotes rapid growth and epithelial tissue necrosis during intestinal infection. PLoS Pathog **8:**e1002581. http://dx.doi.org/10.1371/journal.ppat.1002581.
49. **Lo HR, Lin JH, Chen YH, Chen CL, Shao CP, Lai YC, Hor LI.** 2011. RTX toxin enhances the survival of *Vibrio vulnificus* during infection by protecting the organism from phagocytosis. J Infect Dis **203:**1866–1874. http://dx.doi.org/10.1093/infdis/jir070.
50. **Wright AC, Morris JG.** 1991. The extracellular cytolysin of *Vibrio vulnificus*: inactivation and relationship to virulence in mice. Infect Immun **59:**192–197.
51. **Schaible UE, Kaufmann SHE.** 2004. Iron and microbial infection. Nat Rev Microbiol **2:**946–953. http://dx.doi.org/10.1038/nrmicro1046.
52. **Weinberg ED.** 2009. Iron availability and infection. Biochim Biophys Acta **1790:**600–605. http://dx.doi.org/10.1016/j.bbagen.2008.07.002.
53. **Murciano C, Hor LI, Amaro C.** 2015. Host-pathogen interactions in *Vibrio vulnificus*: responses of monocytes and vascular endothelial cells to live bacteria. Future Microbiol **10:**471–487. http://dx.doi.org/10.2217/fmb.14.136.
54. **Skaar EP.** 2010. The battle for iron between bacterial pathogens and their vertebrate hosts. PLoS Pathog **6:**e1000949. http://dx.doi.org/10.1371/journal.ppat.1000949.
55. **Arezes J, Jung G, Gabayan V, Valore E, Ruchala P, Gulig PA, Ganz T, Nemeth E, Bulut Y.** 2015. Hepcidin-induced hypoferremia is a critical host defense mechanism against the siderophilic bacterium *Vibrio vulni-*

ficus. Cell Host Microbe **17:**47–57. http://dx.doi.org/10.1016/j.chom.2014.12.001.

56. **Rodionov DA, Hebbeln P, Gelfand MS, Eitinger T.** 2006. Comparative and functional genomic analysis of prokaryotic nickel and cobalt uptake transporters: evidence for a novel group of ATP-binding cassette transporters. J Bacteriol **188:**317–327. http://dx.doi.org/10.1128/JB.188.1.317-327.2006.
57. **Ottemann KM, Miller JF.** 1997. Roles for motility in bacterial-host interactions. Mol Microbiol **24:**1109–1117. http://dx.doi.org/10.1046/j.1365-2958.1997.4281787.x.
58. **Milton DL, O'Toole R, Horstedt P, Wolf-Watz H.** 1996. Flagellin A is essential for the virulence of *Vibrio anguillarum*. J Bacteriol **178:**1310–1319.
59. **Staskawicz B, Dahlbeck D, Keen N, Napoli C.** 1987. Molecular characterization of cloned avirulence genes from race 0 and race 1 of *Pseudomonas syringae* pv. *glycinea.* J Bacteriol **169:**5789–5794.
60. **Ditta G, Stanfield S, Corbin D, Helinski DR.** 1980. Broad host range DNA cloning system for gram-negative bacteria: construction of a gene bank of Rhizobium meliloti. Proc Natl Acad Sci U S A **77:**7347–7351. http://dx.doi.org/10.1073/pnas.77.12.7347.